

See discussions, stats, and author profiles for this publication at: <https://www.researchgate.net/publication/49792988>

# Direct Observation of Macrostructure Formation of Hierarchically Structured Meso-Macroporous Aluminosilicates with 3D Interconnectivity by Optical Microscope

ARTICLE *in* LANGMUIR · MARCH 2011

Impact Factor: 4.46 · DOI: 10.1021/la104679h · Source: PubMed

---

CITATIONS

16

READS

45

## 4 AUTHORS, INCLUDING:



Arnaud Lemaire

University of Namur

10 PUBLICATIONS 253 CITATIONS

[SEE PROFILE](#)



Joanna C. Rooke

University of Namur

45 PUBLICATIONS 799 CITATIONS

[SEE PROFILE](#)



Li-Hua Chen

Wuhan University of Technology

24 PUBLICATIONS 345 CITATIONS

[SEE PROFILE](#)

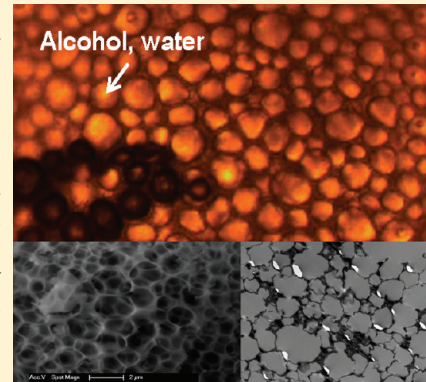
## Direct Observation of Macrostructure Formation of Hierarchically Structured Meso–Macroporous Aluminosilicates with 3D Interconnectivity by Optical Microscope

Arnaud Lemaire,<sup>†</sup> Joanna Claire Rooke,<sup>†</sup> Li-Hua Chen,<sup>†</sup> and Bao-Lian Su<sup>\*,†,‡</sup>

<sup>†</sup>Laboratory of Inorganic Materials Chemistry (CMI), University of Namur (FUNDP), 61 rue de Bruxelles, 5000 Namur, Belgium

<sup>‡</sup>State Key Laboratory of Advanced Technology for Materials Synthesis and Processing, Wuhan University of Technology, 122 Luoshi Road, 430070, Wuhan, Hubei, China

**ABSTRACT:** Hierarchically structured spongy meso–macroporous aluminosilicates with high tetrahedral aluminum content were synthesized from a mixture of single molecular alkoxide precursor,  $(\text{sec-BuO})_2\text{-Al-O-Si(OEt)}_3$ , already containing Si–O–Al bonds, and a silica coreactant, tetramethoxysilane (TMOS). The spontaneous byproduct templated macroporous structure formation has been directly visualized using *in situ* high-resolution optical microscopy (OM), allowing the crucial observation of a microbubble dispersion which is directly correlated to the macrostructure observed by electronic microscopies (SEM and TEM). This discovery leads to a comparative study with meso–macroporous pure metal oxide and to a proposal of the formation mechanism of meso–macroporous aluminosilicates with 3D interconnectivity. The aluminosilicate phase/microbubbles emulsion is produced by a phase separation process occurring between the aluminosilicate nanoparticles and the liquid hydrolysis–condensation reaction byproducts (water, methanol, ethanol, and butanol). The use of alkoxysilane improves the heterocondensation rates between the highly reactive aluminum alkoxide part of the single precursor and added silica species but, above all, leads to the spontaneous generation of an unusual meso–macroporosity in alkaline media. The particles obtained at pH = 13.0 featured regular micrometer-sized macrospheres separated by very thin mesoporous walls and connected by submicrometric openings, providing a 3D interconnectivity. The slight increase in pH value to 13.5 induced significant modifications in morphology and textural properties due to the slower gelification process of the aluminosilicate phase, resulting in the formation of an aluminosilicate material constituted of 1–2  $\mu\text{m}$  large independent hollow mesoporous spheres.



### 1. INTRODUCTION

Recent studies demonstrated the high superiority of meso–macrostructured catalysts in a large series of catalytical reactions and made significant advances in the concrete applications of meso–macroporous materials.<sup>1</sup> Integrating macroporosity in catalytic materials can permit better mass transfer to the active sites situated in the micro- and mesopores that are contained within the material's walls, especially when large molecules are used.<sup>2–5</sup> Several strategies have been developed to achieve this goal by using either polymeric beads and silica opals,<sup>6</sup> postsynthesis,<sup>7</sup> a soft sacrificial template,<sup>8</sup> foam,<sup>9</sup> emulsions,<sup>10</sup> ice crystals,<sup>11</sup> or even replication of natural structures<sup>12</sup> such as bacterial threads<sup>13</sup> with the combination of amphiphilic molecules to generate hierarchically bimodal porous materials. Nevertheless, these syntheses are quite tedious, and the extraction of templates is problematic, leading to the formation of important defects in the structure. Thus, a homogeneous and interconnected hierarchical porosity is difficult to achieve. Recently, a self-formation phenomenon of porous hierarchy, leading to a new alkoxide-based synthesis pathway which yields spontaneously hierarchical meso–macroporosity within oxide materials and without the need of any physical templating agent, has been described.<sup>3–5,12,14</sup> The structure, containing multiple porosities in different length scales, can be

autogenerated by the rapid release of alcohol and water acting as a porogen, during the fast reactions of hydrolysis and polycondensation. This efficient and practical reaction pathway was successfully employed in the conception of macro–meso–microporous oxides (i.e.,  $\text{ZrO}_2$ ,  $\text{TiO}_2$ ,  $\text{Nb}_2\text{O}_5$ ,  $\text{Y}_2\text{O}_3$ ,  $\text{Al}_2\text{O}_3$ ) and mixed oxides and applied to prepare efficient catalysts.<sup>15</sup> This method has been recently extended to the utilization of alkylmetals as precursors releasing gas molecules, which can be used as porogen, to generate a 3D meso–macroporous foamlke framework.<sup>16</sup>

Aluminosilicates are one of the most important chemical compositions used in industry as catalyst, catalyst support, adsorbent, etc. For example, amorphous aluminosilicates are largely used as support for FCC catalysts. The introduction of a three length scaled macro–meso–microporosity into aluminosilicate materials will largely improve the performance in catalysis and separation from a diffusion point of view. Hierarchically meso–macroporous aluminosilicates have been prepared by using two independent precursors  $\text{Al}(\text{OBu})_3$  and TMOS on the basis of a self-formation strategy. The materials obtained are composed of

**Received:** November 24, 2010

**Revised:** January 3, 2011

**Published:** January 28, 2011

well-organized parallel macrochannels of funnel-like shape.<sup>3a,5</sup> A large mesoporosity was generated by aggregates of particles of several tens of nanometers which are themselves formed by the aggregation of nanometric particles, resulting in a very homogeneous mesoporosity of several nanometers. These kinds of features are quite desirable for use in industry. However, the utilization of two independent precursors led unavoidably to the heterogeneity in final materials. Indeed, due to the difference in reactivity of  $\text{Al}(\text{BuO})_3$  and TMOS, the homocondensation reactions between hydrolyzed aluminum alkoxide molecules conducts to the large formation of Al—O—Al linkages. The heterocondensation reactions between hydrolyzed aluminum alkoxide and TMOS are not favored. The synthesized materials consist of a mixture of aluminosilicate and  $\text{Al}_2\text{O}_3$  with high content of extra-framework Al. This is not favorable for activity and selectivity during catalytic processes. The single molecular precursor  $(\text{Bu}^{\circ}\text{O})_2\text{Al—O—Si(OEt)}_3$ , featuring a preformed Al—O—Si linkage, has been used in the synthesis of highly ordered mesoporous aluminosilicate with a Si/Al ratio close to 1<sup>17a</sup> and hierarchically meso—macroporous aluminosilicates with 3D interconnectivity.<sup>17b</sup> This molecular source possesses two alkoxide functionalities that should undergo fast hydrolysis and polycondensation reactions, allowing the self-generation of a hierarchical macro—mesoporosity. By using tetraalkoxysilane (TEOS, TPOS, TBOS, or a mixture of TMOS and TEOS)<sup>18</sup> or chelating agents such as carboxylate salts,<sup>17b</sup> the rupture of the Al—O—Si linkage was partially prevented, and the Si/Al ratios of the final materials obtained can be adjusted close to the unit. More interestingly, instead of the formation of parallel funnel-like macrochannels through the synthesized particles, usually obtained on the basis of self-formation strategy, the produced materials featured outstanding disordered macrochannels<sup>17b</sup> or spongy macrostructures with regular micro-sized hollow spheres, displaying 3D interconnections.<sup>18</sup> This kind of structures, combining variable Si/Al ratios and very high amount of intraframework Al species, are quite suited for catalysis and separation applications.

Some comprehensive studies on the generation of hierarchically meso—macroporous metal oxides, with parallel funnel-like macrochannels and via the self-formation strategy, lead to the deep understanding on the formation mechanism.<sup>3</sup> The quite intriguing and different macrostructures obtained when using a single molecular precursor with two alkoxide functionalities, such as  $(\text{Bu}^{\circ}\text{O})_2\text{Al—O—Si(OEt)}_3$ , compared to those using one single metal alkoxide or a mixture of two independent alkoxides should result from the difference of the polymerization rate of alkoxide precursors. Recently, an optical microscope has been successfully used to follow the macrostructure formation and demonstrated its great potential to study the self-formation mechanism of meso—macroporous materials from the aqueous polymerization of metal alkoxides.<sup>3</sup>

The present work reports a comprehensive study on the formation mechanism of hierarchically meso—macroporous aluminosilicate materials using single source molecular precursor,  $(\text{Bu}^{\circ}\text{O})_2\text{Al—O—Si(OEt)}_3$ , with TMOS as a silicon coreactant. This has been achieved on the basis of the direct observation of the macrostructure formation, within the aluminosilicate polymerizing phase, by using optical microscopy (OM). This study, throughout the variation of the pH value of solutions, also highlights the strong influence of the acido-basicity of the synthetic media on this meso—macroporous self-formation phenomenon. The better understanding of the formation mechanism can allow us to develop more efficient synthesis procedures to aluminosilicate materials with desired macrostructures and advanced functionalities.

**Table 1. Names, pH Conditions, and Textural Properties of the Synthesized Aluminosilicate Materials**

samples	pH	Al—Si ester/ TMOS	$S_{\text{BET}}$ ( $\text{m}^2/\text{g}$ )	$V_p$ ( $\text{cm}^3/\text{g}$ )	$\varnothing$ (nm)
Al—Si-2	2.0	/	384	0.4	2–6
Al—Si-6.5	6.5	/	453	0.6	3–7
Al—Si-13	13.0	/	318	0.5	3 and 35
Al—Si-13.5	13.5	/	219	0.4	1.5
Al—Si-TM2	2.0	1/1	315	0.5	1–10
Al—Si-TM6.5	6.5	1/1	269	0.6	2–10
Al—Si-TM13	13.0	1/1	315	0.6	5
Al—Si-TM13.5	13.5	1/1	126	0.5	<1.5 and 5–15

## 2. EXPERIMENTAL SECTION

**2.1. Preparation of Meso—Macroporous Materials.** The Al—Si ester, di-*s*-butoxyaluminoxytriethoxysilane ( $(\text{Bu}^{\circ}\text{O})_2\text{Al—O—Si(OEt)}_3$ ), was purchased from Gelest, and other chemicals were purchased from Aldrich. They were used without any further purification. Acidic solution at pH 2.0 was prepared by using HCl 37%, whereas aqueous alkaline solutions (pH = 13.0 and 13.5) were prepared by dissolving NaOH in 60 mL of bidistilled water (at a pH of 6.5). For the study of the effect of pH values in the absence of silica coreactant, 5.0 g of the Al—Si ester was dropwise added to the pH-adjusted solutions (pH = 2.0, 6.5, 13.0, and 13.5, respectively) under very mild stirring (<100 rpm). After 1 h, the mixture was transferred into a Teflon-lined autoclave and heated to 80 °C for 24 h. The solid products were filtered, washed with water, and dried in an oven at 40 °C. These samples prepared at pH of 2.0, 6.5, 13.0, or 13.5 are, respectively, named Al—Si-2, Al—Si-6.5, Al—Si-13, and Al—Si-13.5. To synthesis hierarchical 3D meso—macroporous aluminosilicates, 5.0 g of the Al—Si ester was mixed intimately with 2.2 g of tetramethoxysilane (TMOS) (molar ratios Al—Si ester/TMOS = 1:1) under vigorous stirring (700 rpm) for 5 min. The mixture was slowly added dropwise into pH adjusted solutions (pH = 2.0, pH = 6.5, pH 13.0 and 13.5) under very mild stirring (<100 rpm). After 1 h the mixture was transferred into a Teflon-lined autoclave and heated to 80 °C for 24 h. Solid products were filtered, washed, and dried (40 °C). Materials obtained from the mixture of the single molecular precursor and TMOS as coreactant are labeled as Al—Si—TM. The number following immediately Al—Si—TM prefixes indicates the pH value used for the synthesis. Solutions at pH of 2.0, 6.5, 13.0, or 13.5 correspond, respectively, to Al—Si—TM2, Al—Si—TM6.5, Al—Si—TM13, and Al—Si—TM13.5 materials. All the information is detailed in Table 1.

The meso—macroporous aluminosilicate solid with parallel straight macrochannels was prepared, as a reference sample for the macrostructure comparison, by using a mixture of two independent metal alkoxide precursors ( $\text{Al}(\text{O}^{\circ}\text{Bu})_3$  and TMOS in a 1/1 molar ratio), following the preparation pathway previously reported.<sup>3–5</sup>

**2.2. Characterization.** Transmission electronic microscopy (TEM) experiments were performed on a Philips TECNAI-10 microscope at an acceleration voltage of 80 kV with sample powders embedded in an epoxy resin and sectioned with an ultramicrotome. The  $\text{N}_2$  adsorption and desorption isotherms were measured at −196 °C with a volumetric adsorption analyzer, Micromeritics Tristar 3000. The morphology as well as the macroporous array were studied using a Philips XL-20 scanning electron microscope (SEM) and a JEOL JSM 7500 field emission scanning electron microscope (FE-SEM) with conventional sample preparation and imaging techniques. The environments of the Al and Si atoms were studied via  $^{27}\text{Al}$  MAS NMR and  $^{29}\text{Si}$  MAS NMR, respectively, with a Bruker Avance 500 spectrometer. For all the measurements, we used magic angle spinning ( $\theta = 54.7^\circ$ ). For the  $^{29}\text{Si}$  MAS NMR, the standard measurements were made with a pulse angle of 30° and a recycling delay of 6 s. Concerning  $^{27}\text{Al}$  MAS NMR, the pulse angle

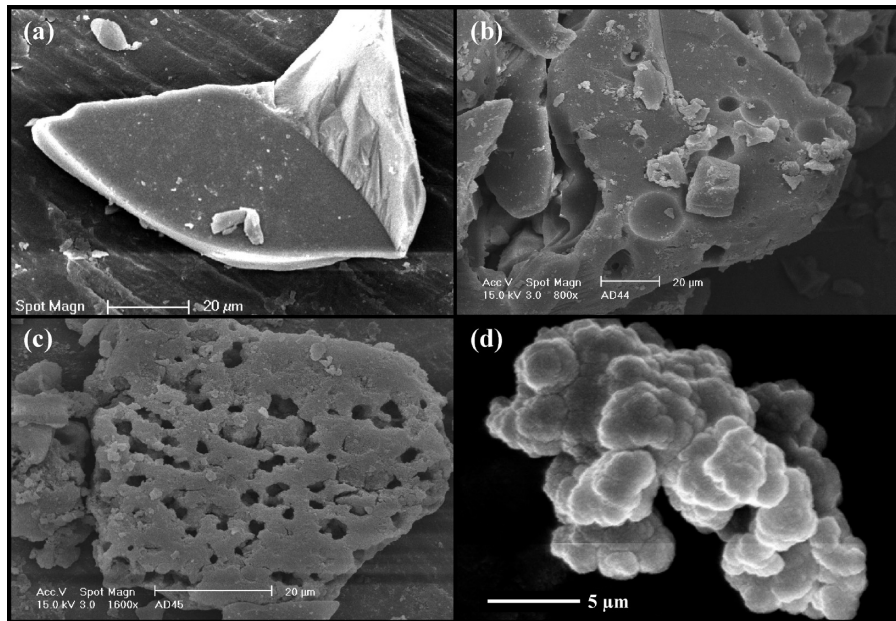


**Figure 1.** SEM images of reference sample aluminosilicate particles synthesized at different pH values (2.0, 6.5, 13.0, and 13.5), with the di-s-butoxyaluminoxytriethoxysilane single precursor without any silica coreactant: (a) Al-Si-2, (b) Al-Si-6.5, (c) Al-Si-13, and (d) Al-Si-13.5.

is  $10^\circ$  with  $t$  pulse =  $1\ \mu$ s and a recycling delay of 0.1 s. The global Si/Al ratio was investigated with the help of a Philips PU9200X atomic absorption spectrometer.

**2.3. Direct Observation of the Macrostructure Formation by Optical Microscopy.** Optical microscopic (OM) investigations were performed by the use of a KOLLEG SHB45, and images were recorded by a Moticam 1000 camera connected to the ocular. Observations started as soon as a  $20\ \mu\text{L}$  Al-Si ester/TMOS mixture droplet was deposited on an aqueous thin film at fixed pH (pH of 2.0, 6.5, 13.0, or 13.5) covering an observation glass slide.

### 3. RESULTS AND DISCUSSION

**3.1. Morphology and Pore Organization.** The morphological structure and the pore organization of the materials prepared from the single molecular Al-Si ester ( $(\text{Bu}^{\circ}\text{O})_2\text{Al}-\text{O}-\text{Si}(\text{OEt})_3$ ) and from the mixture of Al-Si ester/TMOS with a ratio of 1/1 at pH 2.0, 6.5, 13.0, and 13.5 were directly visualized by SEM and TEM.

**Synthesis with Al-Si Ester at Different pH Values.** As it is visible on the SEM pictures in Figure 1a–d, materials prepared at different pH values exhibit particles of ca.  $20\text{--}40\ \mu\text{m}$  with smooth surfaces, albeit the sample synthesized at pH 13.0 (Al-Si-13, Figure 1c) exhibits some very disordered micro-sized openings. All the above SEM observations are well confirmed by TEM study (Figure 2). In fact, TEM pictures of the materials synthesized at a pH of 2.0, 6.5, and 13.5 (Al-Si-2, Al-Si-6.5, and Al-Si-13.5 in Figure 2 a, b, and d, respectively) do not show any macroporous structure inside particles; only a vermicular mesoporosity, certainly produced by the aggregation of aluminosilicate nanoparticles, is observed.<sup>3</sup> However, the Al-Si-13 sample possesses some particles presenting a disordered macrostructure (Figure 2c) constituted of irregular macrochannels and separated by mesoporous walls (Figure 2c, inset).

**Synthesis with the Mixture of the Al-Si Ester and TMOS at Different pH Values.** Figure 3a–d depicts SEM pictures of materials prepared at a pH of 2.0, 6.5, 13.0, and 13.5, respectively,

from mixtures of Al-Si ester and TMOS. Its macrostructured particles can only be obtained at pH values ranging from 13.0 (Figure 3c) to 13.5 (Figure 3d). The Al-Si-TM13 sample is integrally constituted of very large highly spongy particles of ca.  $60\text{--}80\ \mu\text{m}$  which are comprised of very regular micrometer-sized macrovoids. There are many of these  $1\text{--}2\ \mu\text{m}$  spherical voids, which are separated by thin walls and are found over the entire surface of the particle as well as within the particle. These first results show that the introduction of TMOS as coreactant, coupled with high pH value, is essential to generate the macro-scaffold. Al-Si-TM13 material also exhibits some interconnections between spherical voids due to the very thin walls separating each spherical cavity (inset of Figure 3c). Surprisingly, only a slight increase in the pH value of the synthetic media induces a significant change in the morphology of particles. Figure 3d represents the SEM image of the material prepared at pH 13.5 (Al-Si-TM13.5) and shows that the macrostructure consists in the stacking of micro-sized ( $1\text{--}2\ \mu\text{m}$  diameter) hollow spheres. The picture in the inset of Figure 3d shows fully independent hollow spheres. No macrostructures are observed for the two other materials (Al-Si-TM2 and Al-Si-TM6.5 in Figure 3a and b, respectively). These observations are also established by TEM analysis.

TEM images of the samples synthesized from the mixture of Al-Si ester and TMOS are exhibited in Figure 4. Materials prepared with TMOS at pH values of 2.0 and 6.5 (Al-Si-TM2 and Al-Si-TM6.5, Figure 4a and b, respectively) are not macroporous and characterized by a disordered mesoporosity. In the case of the Al-Si-TM13 aluminosilicate, prepared at pH 13.0, the TEM image (Figure 4c) highlights circular openings of  $\sim 2\ \mu\text{m}$  large, surrounded by very thin walls of about  $100\text{--}400\ \text{nm}$  thickness. A deeper look into the structure reveals a vermicular mesoporosity contained in the macrowalls separating macrovoids (inset of Figure 4c). Figure 4d presents the case of the material prepared at pH = 13.5 (Al-Si-TM13.5). The TEM picture in Figure 4d exposes a macroporous array which is comprised of spherical voids separated by even thinner walls.

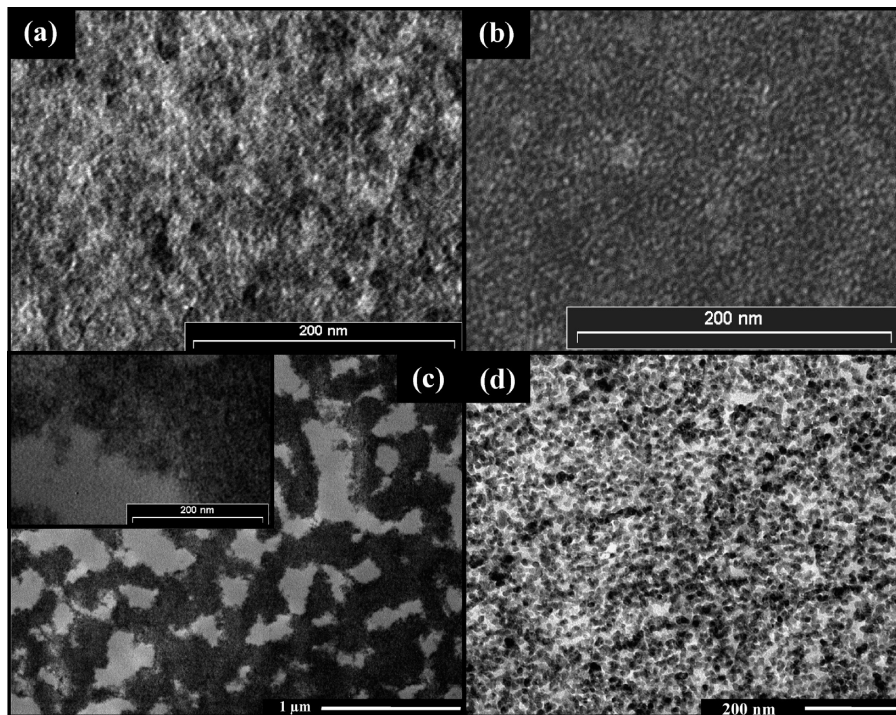


**Figure 2.** Cross-sectional transmission electron microscopy (TEM) images of the aluminosilicate materials synthesized at different pH values (2.0, 6.5, 13.0, and 13.5), with the di-*s*-butoxyaluminoxytriethoxysilane single precursor without any silica coreactant: (a) Al–Si-2, (b) Al–Si-6.5, (c) Al–Si-13, and (d) Al–Si-13.5.

In certain areas, there is a great abundance of voids with connections arising between some of them. Macroporous material seems to be constructed by the stacking of independent and spherically shaped macrovoids of about 0.1–1  $\mu\text{m}$  large, which is confirmed by SEM investigations (Figure 3d). A high-magnification TEM image (inset of Figure 4d) of the cross-sectional aluminosilicate Al–Si-TM13.5 specimen also reveals that these thin macroporous walls are composed of accessible disordered mesoporous arrays generated by the assembly of particles. Moreover, material prepared at pH 13.5 shows cavities between the stacked mesoporous aluminosilicate nanoparticles of 50 nm length, which could suggest a further interparticular porosity.

**3.2. Textural Properties.** All the nitrogen adsorption–desorption isotherms and corresponding pore size distributions of the samples, synthesized in both the presence and the absence of silica coreactant, are shown in Figure 5. Textural properties such as accessible surface areas ( $S_{\text{BET}}$ ), pore volumes ( $V_p$ ), and pore sizes ( $\bar{\phi}$ ) are listed in Table 1.

*Synthesis with Al–Si Ester at Different pH Values.* The samples Al–Si-2 and Al–Si-6.5 (Figure 5a and b) display classical type IV isotherms. These two isotherms are presenting traditional textural characteristics of aluminosilicate materials prepared from alkoxide precursors, without any mesoscopic templating agents. These materials feature accessible surface area around 400  $\text{m}^2/\text{g}$ , pore volume about 0.5  $\text{cm}^3/\text{g}$ , and very homogeneous pore size distribution centered at 4 and 5 nm, respectively. These results are in total agreement with the observations made by TEM (Figure 2a and b, respectively). In the case of Al–Si-13 and Al–Si-13.5 samples, two interesting inflections are visible on corresponding isotherms (Figure 5c and d, respectively). The samples first undergo a capillary condensation step at a relative pressure ( $p/p_0$ ) of about 0.60, indicating the presence

of mesopores. A second capillary condensation step occurs at very high relative pressure ( $p/p_0 \geq 0.9$ ), which is evidence of an appreciable amount of secondary porosity, resulting probably from interparticular porosity. The analysis of the pore size distributions of the Al–Si-13 specimen (Figure 5c), calculated by the Barret–Joyner–Halenda (BJH) method from the adsorption branch of the isotherm, reveals first a relatively narrow porous system centered around 3 nm, which is confirmed by TEM observations (Figure 2c, inset), and a second broader one, located at around 35 nm (Figure 5c), which is also confirmed by TEM observations (Figure 2c). The BJH pore size distribution of the Al–Si-13.5 material exhibits a narrow peak centered at 2.5 nm (Figure 5d) and a very broad second pore size distribution with no apparent maximum, due to the technique limits of the  $\text{N}_2$  adsorption–desorption apparatus. The specific surface areas, reported in Table 1, have been calculated by the BET method giving 318 (Al–Si-13) and 219  $\text{m}^2/\text{g}$  (Al–Si-13.5), respectively.

*Synthesis with the Mixture of Al–Si Ester and TMOS at Different pH Values.* When a mixture of di-*s*-butoxyaluminoxytriethoxysilane and TMOS is used in an aqueous media, important modifications of textural properties are recorded. Indeed, for instance, isotherms of materials prepared from a di-*s*-butoxyaluminoxytriethoxysilane and TMOS mixture, at pH of 2.0 and 6.5 (named Al–Si-TM2, Figure 5e, and Al–Si-TM6.5, Figure 5f), are transformed to type II, testifying the existence of an additional porosity. Textural properties of these two materials are listed in Table 1. More interestingly, the isotherm of the Al–Si-TM13 sample, exhibited in Figure 5g, is similar to type IV, characteristic of mesoporous compounds. A capillary condensation step can be seen at relative pressures of around 0.75 indicating the presence of large mesopores. From these data sets, pore size distributions are calculated with maxima centered at ~5 nm (Figure 5g), which has been observed by

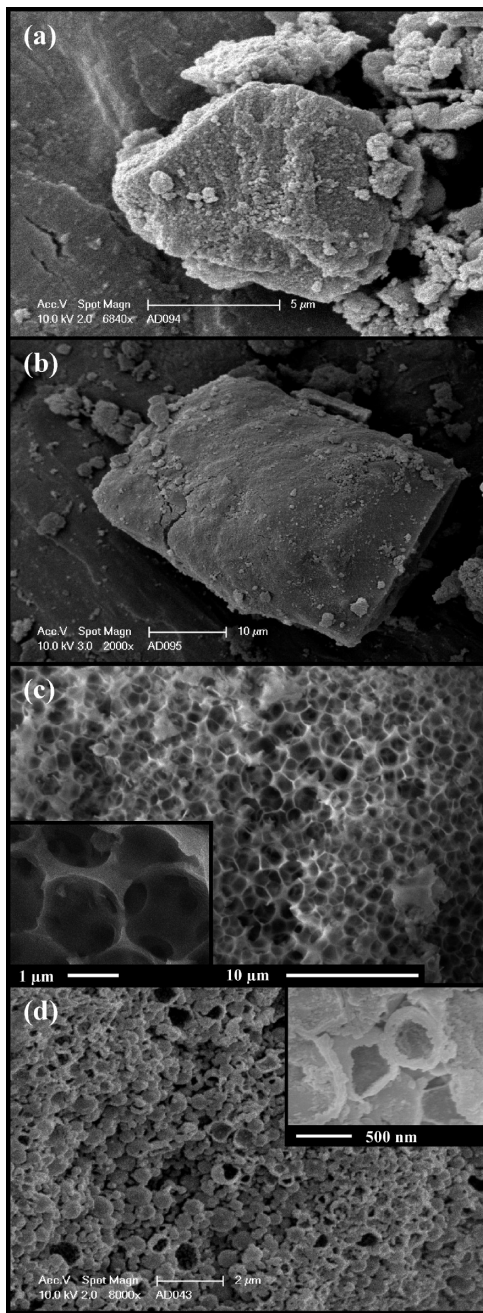


**Figure 3.** SEM images of sample aluminosilicate particles synthesized at different pH values (2.0, 6.5, 13.0, and 13.5), with the di-*s*-butoxyaluminoxytriethoxysilane single precursor and TMOS as silica coreactant in a 1:1 di-*s*-butoxyaluminoxytriethoxysilane/TMOS ratio: (a) Al—Si—TM2, (b) Al—Si—TM6.5, (c) Al—Si—TM13, and (d) Al—Si—TM13.5.

TEM (Figure 4c, inset). Al—Si—TM13 material has a very high specific surface area (see Table 1), which is  $315\text{ m}^2/\text{g}$ . Aluminosilicate material synthesized in the more alkaline solution (pH 13.5) with TMOS presents a macroporous type II isotherm (Figure 5h). This confirms again the presence of a larger porosity observed by TEM (Figure 4c, inset). The specific surface area, reported in Table 1, is  $126\text{ m}^2/\text{g}$ . All the aluminosilicate samples investigated present pore volumes of around  $0.5\text{ cm}^3/\text{g}$ . The tendency observed in surface area of materials obtained as a function of pH value of the synthesis system is in good agreement with sol–gel chemistry. In

general, for a silicate precursor, under acidic conditions, the hydrolysis rate is higher than that of condensation, and more hydrolyzed monomers are formed yielding linear or randomly branched polymers with a micro- or mesoporosity and a higher surface area. However, base-catalyzed hydrolysis and polycondensation led to highly branched polymeric gel, giving a larger porosity with a lower surface area.<sup>19</sup> The great originality of the present work is to create two porosities simultaneously in one solid body by using the single molecular alkoxide precursor, (*sec*-BuO)<sub>2</sub>—Al—O—Si(OEt)<sub>3</sub>, and a silica coreactant, TMOS.

### 3.3. Al and Si Chemical Environments and Si/Al Ratios by Solid State $^{27}\text{Al}$ and $^{29}\text{Si}$ MAS NMR and Elemental Analysis.

The acidic properties and catalytic activity of aluminosilicate materials are generally produced by the presence of trivalent Al atoms in the silica framework. The coordination environments of Al atoms in the samples were characterized by  $^{27}\text{Al}$  MAS NMR, and spectra are exhibited in Figure 6. This method combined with elemental analysis (Table 2, measured by atomic absorption spectrometry) yields the silica to aluminum ratios (Si/Al) and silica to tetrahedral aluminum ratio (Si/Al<sub>T</sub>, ratio only considering tetrahedral aluminum (Al<sub>T</sub>) incorporated into the tetrahedral silicated framework). All the  $^{27}\text{Al}$  NMR spectra of the aluminosilicate materials exhibit one peak at  $\sim 58\text{ ppm}$  and another one around 3–6 ppm, corresponding, respectively, to tetrahedrally coordinated framework aluminum species and octahedrally extra framework aluminum species.

*Synthesis with Al—Si Ester at Different pH Values.* The increase in pH clearly favors the incorporation of tetrahedral aluminum species into the framework as shown by the superposition of spectra of materials prepared at different pH values, in Figure 6(A). An elevation in the pH of the media from 2.0 to 13.5 (Figure 6(A)) results generally in a major increase in tetrahedral aluminum and thus a decrease in the Si/Al<sub>T</sub> ratios (Table 2). This trend can be explained in terms of pH. Basic media reduces the aluminum polymerization rate, such that the alkoxy silane polymerization rate is of a similar value, and thus the two polymerization reactions are in competition. Further explanation lies in the fact that the high concentration of OH<sup>−</sup> anions displaces the equilibrium of the octahedrally coordinated aluminum species in favor of [AlOH]<sub>4</sub><sup>−</sup>, thus the tetrahedral anion becomes the thermodynamically favorable species and is preferably incorporated within a tetrahedral framework rather than the octahedral Al(H<sub>2</sub>O)<sub>6</sub><sup>3+</sup> species.<sup>19</sup> Otherwise, acidic or neutral medias, such as for the preparation of Al—Si-2 and Al—Si-6.5 materials (Figure 6(A)a and b and Table 2), result in very poor incorporation of aluminum into the framework.

*Synthesis with the Mixture of Al—Si Ester and TMOS at Different pH Values.* Addition of silica inorganic coreactant enhances the predominance of tetrahedrally coordinated aluminum species regardless of the initial pH value, as can be seen in Figure 6(B), by the  $^{27}\text{Al}$  NMR MAS spectra superposition of materials prepared at different pH values ranging from 2.0 to 13.5 in the presence of TMOS. These spectra are all showing that a higher part of the aluminum is in tetrahedral configuration, meaning a significant increase of aluminum incorporation into the silicated framework. Al—Si—TM13.5 material is only constituted of intraframework Al species. When a mixture of di-*s*-butoxyaluminoxytriethoxysilane and silica coreactant is added to an aqueous media, the likelihood that polymerization occurs between an aluminum site and a silicon

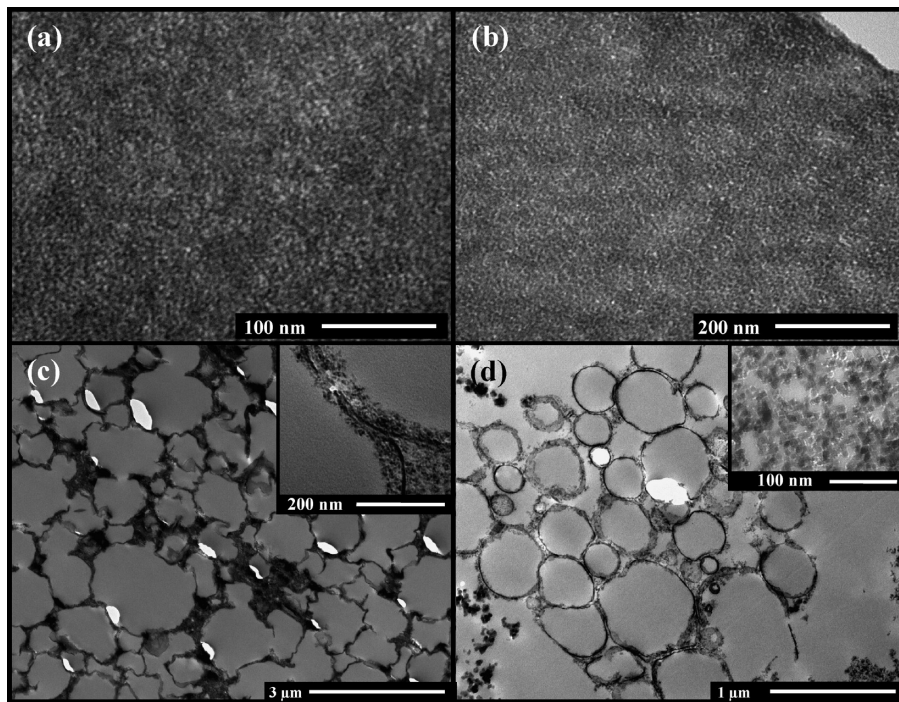


**Figure 4.** Cross-sectional transmission electron microscopy (TEM) images of the aluminosilicate particles synthesized at different pH values (2.0, 6.5, 13.0, and 13.5), with the di-*s*-butoxyaluminoxytriethoxysilane single precursor and TMOS as silica coreactant: (a) Al–Si–TM2, (b) Al–Si–TM6.5, (c) Al–Si–TM13, and (d) Al–Si–TM13.5.

site ( $\text{Al}–\text{O}–\text{Si}$ ) instead of  $\text{Al}–\text{O}–\text{Al}$  linkages is increased, implying the reduction in the rupture of  $\text{Al}–\text{O}–\text{Si}$  linkages of the single molecular precursor. This is due to the additional alkoxy functional groups in TMOS, creating alkoxy bridging between the single-source precursor and the silicon alkoxide. The rich environment of alkoxy silane functional groups around the aluminum nucleophilic center favors heteropolymerization reactions and, consequently, the construction of an  $\text{Al}–\text{O}–\text{Si}$  linkage network. Addition of TMOS at pH of 13.0 (Figure 6(B)c) allows an increase of about 10% more of aluminum into the tetrahedral silicate framework in regard to Al–Si-13 material (Figure 6(A)c). The same trend is observed at pH 13.5, for which almost all the aluminum is tetrahedrally coordinated (Figure 6(B)d). This pH value yield materials only constituted of tetrahedrally coordinated aluminum atoms, and the resulting products are pure homogeneous aluminosilicate materials. Again, in comparison to the material Al–Si-13.5 (Figure 6(A)d) prepared without TMOS, a significant increase (more than 20%) of tetrahedral aluminum content is observed. Moreover, at pH 13.5, lower Si/Al and Si/ $\text{Al}_T$  ratios are obtained in comparison to a Si/Al ratio of the initial gel or the materials prepared at more acidic pH. It is believed that at such elevated pH values soluble stable dimeric silica species  $[(\text{HO})_2\text{Si}(\text{O})–\text{OSi}(\text{O})_2(\text{OH})]^{3-}$  are formed in the synthesis solution and are eliminated from the media after the filtration step.

For more accurate confirmations about the  $\text{Al}–\text{O}–\text{Si}$  repartition into synthesized aluminosilicate materials, the chemical environment of Si was studied by  $^{29}\text{Si}$  MAS NMR investigations (Figure 7). The  $^{29}\text{Si}$  NMR spectrum of the Al–Si–TM13.5 intraframework Al-rich material is presented in Figure 7a and is compared to the  $^{29}\text{Si}$  NMR spectrum of a pure silica material,<sup>20</sup> in Figure 7b. In contrast to this pure silica material, the

aluminosilicate material is showing evidence of the significant shift toward the lower field, such as low silica content zeolites do. The  $^{29}\text{Si}$  NMR spectrum of the material, Al–Si–TM13.5 (Figure 7a), is constituted of a main peak, spreading from –75 to –105 ppm and midpointed at –87 ppm. It is well-known that aluminum species in aluminosilicate materials have specific chemical displacements toward low field:  $\text{Si}(\text{OAl})_4$  at –85 ppm,  $-\text{Si}(\text{OAl})_3$  at –90 ppm,  $=\text{Si}(\text{OAl})_2$  at –95 ppm, and  $\equiv\text{Si}(\text{OAl})_1$  at –100 ppm.<sup>21</sup> This indicates that Al–Si–TM13.5 material possesses an appreciable amount of tetrahedral aluminum incorporated into the silicate matrix to give  $\text{Al}–\text{O}–\text{Si}$  linkages. A proposal of decomposition into different contributions for the  $^{29}\text{Si}$  NMR spectrum of the sample Al–Si–TM13.5 is also presented in Figure 7a. The observed signal seems to result from the contribution of two peaks, one centered at –85 ppm ( $\text{Si}(\text{OAl})_4$ ) and the second at –90 ppm ( $-\text{Si}(\text{OAl})_3$ ). This proposal is in good agreement with Si/Al ratios, provided by elemental analysis, which are close but not exactly equal to 1.0 (Si/Al  $\sim$  1.5). The absence of the signal corresponding to  $\text{Si}(\text{OSi})_4$  indicates clearly that the incorporation of Al in the structure, i.e., heterocondensation between Al alkoxide functionality and that of Si, is highly favored, in particular with higher pH values. The very low Si/ $\text{Al}_T$  obtained (Table 2) confirmed this conclusion.

**3.4. Macrostructure Formation by Optical Microscopy.** Recent studies carried out on the aqueous media synthesis of meso–macroporous materials using metal alkoxides as precursor suggest a mechanism based on the synergy between the polymerization kinetics of the alkoxide precursors and the hydrodynamic flow of the liquids (water and alcohol) released during fast polymerization steps.<sup>3–5,12,14,15</sup> The formation mechanism of highly spongy microvoid shaped meso–macroporous aluminosilicate solid in the present case could be somehow similar but

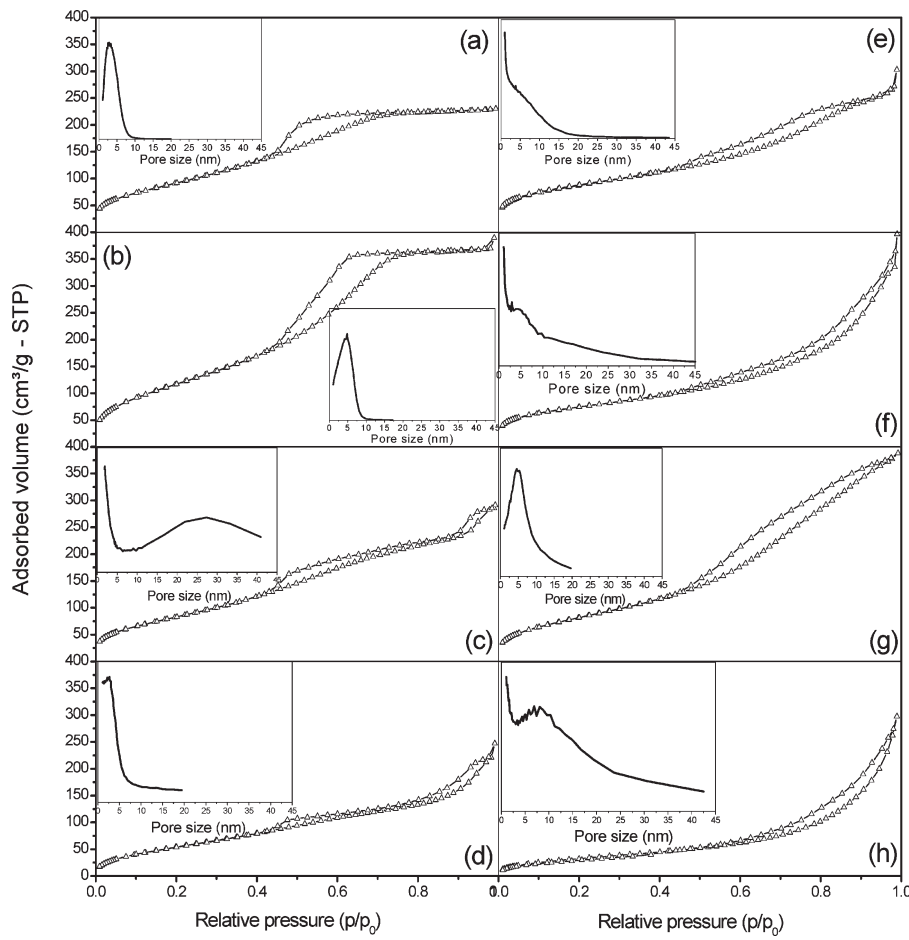


**Figure 5.** N<sub>2</sub> adsorption–desorption isotherms and corresponding pore size distribution of the reference aluminosilicate samples prepared without TMOS: (a) Al–Si-2, (b) Al–Si-6.5, (c) Al–Si-13, and (d) Al–Si-13.5. The samples synthesized in the presence of TMOS: (e) Al–Si–TM2-1, (f) Al–Si–TM6.5-1, (g) Al–Si–TM13-1, and (h) Al–Si–TM13.5.

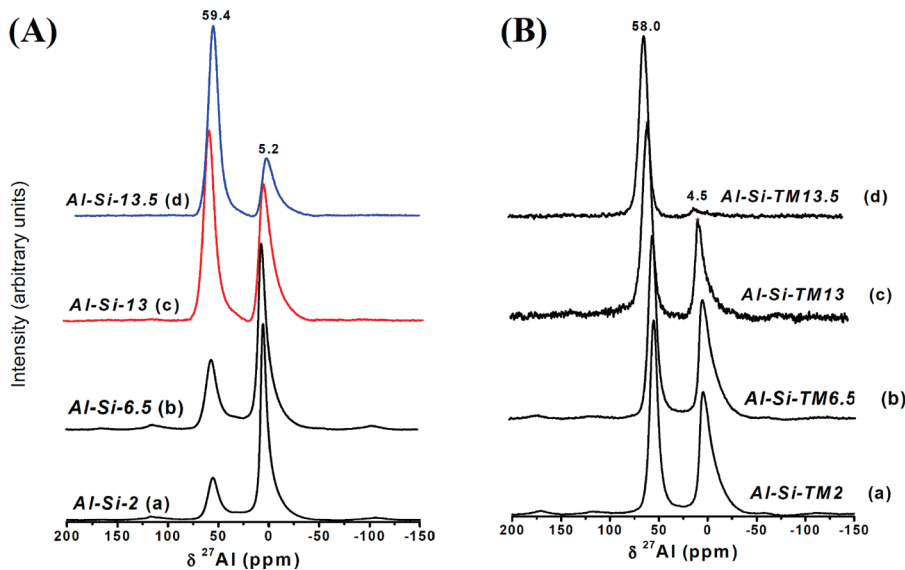


**Figure 6.** <sup>27</sup>Al MAS NMR spectra of reference aluminosilicate samples prepared at (A) varying pH without TMOS: (a) Al–Si-2, (b) Al–Si-6.5, (c) Al–Si-13, and (d) Al–Si-13.5 and (B) with TMOS as silica coreactant at various pH values: (a) Al–Si–TM2-1, (b) Al–Si–TM6.5-1, (c) Al–Si–TM13-1, and (d) Al–Si–TM13.5-1.

**Table 2. Chemical Compositions and Si/Al Ratios of the Presented Aluminosilicate Materials Made by  $^{27}\text{Al}$  and  $^{29}\text{Si}$  MAS NMR and Elemental Analysis**

samples	pH	TMOS	Al—Si ester/ Si/Al	% Al <sub>T</sub>	% Al <sub>O</sub>	Si/Al <sub>T</sub>
Al—Si-2	2.0	/	1.1	22.72	77.28	4.8
Al—Si-6.5	6.5	/	1.1	30.92	69.08	3.8
Al—Si-13	13.0	/	0.9	55.71	44.29	1.6
Al—Si-13.5	13.5	/	0.9	74.28	25.72	1.1
Al—Si-TM2	2.0	1/1	2.0	50.63	49.37	4.0
Al—Si-TM6.5	6.5	1/1	2.0	49.58	50.42	4.1
Al—Si-TM13	13.0	1/1	1.5	67.43	32.57	2.2
Al—Si-TM13.5	13.5	1/1	1.5	96.79	3.21	1.6

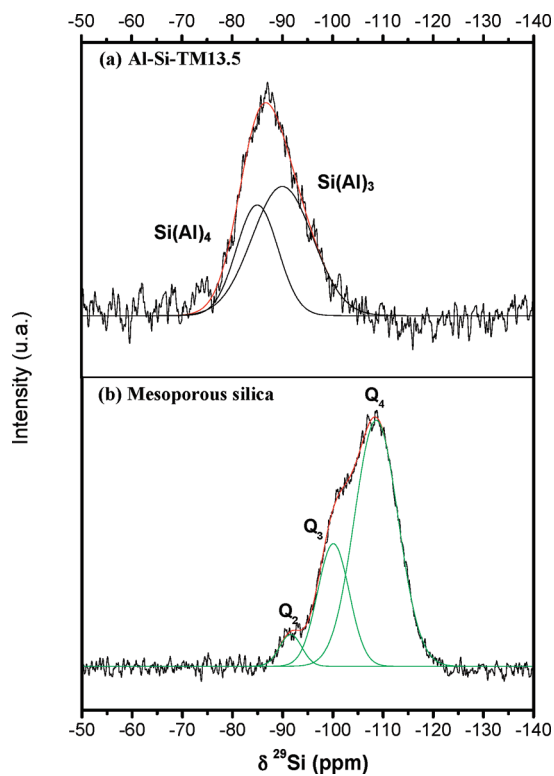


**Figure 7.**  $^{29}\text{Si}$  MAS NMR spectrum of (a) aluminosilicate Al—Si-TM13.5 sample, compared to (b) a pure mesoporous silicated material [ $\text{Q}_2$ :  $=\text{Si}(\text{OSi})_2$ ;  $\text{Q}_3$ :  $-\text{Si}(\text{OSi})_3$ ;  $\text{Q}_4$ :  $\text{Si}(\text{OSi})_4$ ].

more complex compared to the previous one proposed to explain the formation of meso-macroporous materials with quite parallel straight channels crossing the whole particle (Figure 8). Figure 8a depicts an OM image taken during the polymerization process of two independent alkoxide precursors (one droplet of TMOS/ $\text{Al}(\text{OBu})_3$ -based mixture was added onto a pH = 13.0 alkaline solution). The pattern of straight and parallel macrochannels is clearly visible and is confirmed by SEM images (Figure 8b and c). The intimate reason of that statement is due to the fact that in previous cases<sup>3–5,12,14,15</sup> there are only one or a maximum of two alkoxide groups in the reaction system, while in the present case, three alkoxide groups are able to react.

The earlier stage of the Al—Si ester/TMOS-based mixture polymerization was followed by OM observations. Sequential

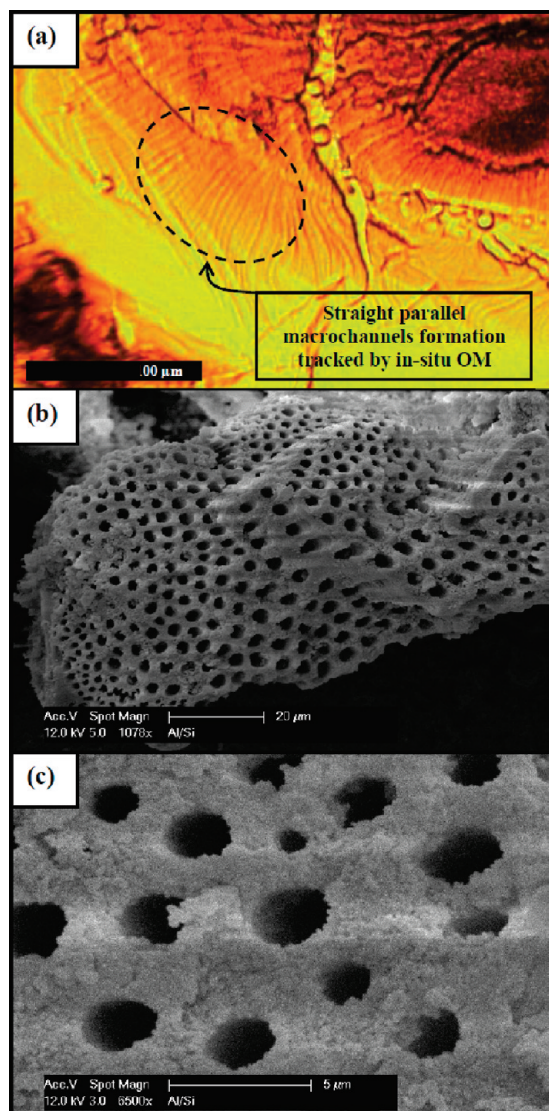


**Figure 8.** OM image (a) and SEM images (b and c) of the tubular, approximately parallel macrochannels formed by the polymerization of two independent silica (TMOS) and aluminum ( $\text{Al}(\text{sOBu})_3$ ) alkoxide precursors.

images (Figure 9) were taken at different reaction times (0 s to 8 min) after the contact of an Al—Si ester/TMOS-based mixture droplet with a pH = 13.0 water film. It is possible to observe that, under these conditions, a darker area (between two white arrows), corresponding to a phase separation process occurring between the liquid phase (production of water and alcohol molecules resulting from hydrolysis) and the inorganic phase (constructed by the condensation of precursors), appears in less than 15 s (Figure 9c).

This phenomenon can be easily observed because it is located at the interface between the water and the droplet of the inorganic phase. The progressive phase separation ends up, in about 20–30 s (Figure 9d), in the formation of independent, mobile, regular, and microsized droplets of liquid ( $\text{H}_2\text{O}$ , butanol, methanol, and ethanol) in this border area. After 45 s (Figure 9e), bubbles spread inside the entire Al—Si ester/TMOS droplet undergoing polymerization. These numerous bubbles slightly grow and gather into moving flows of expanding microdroplets

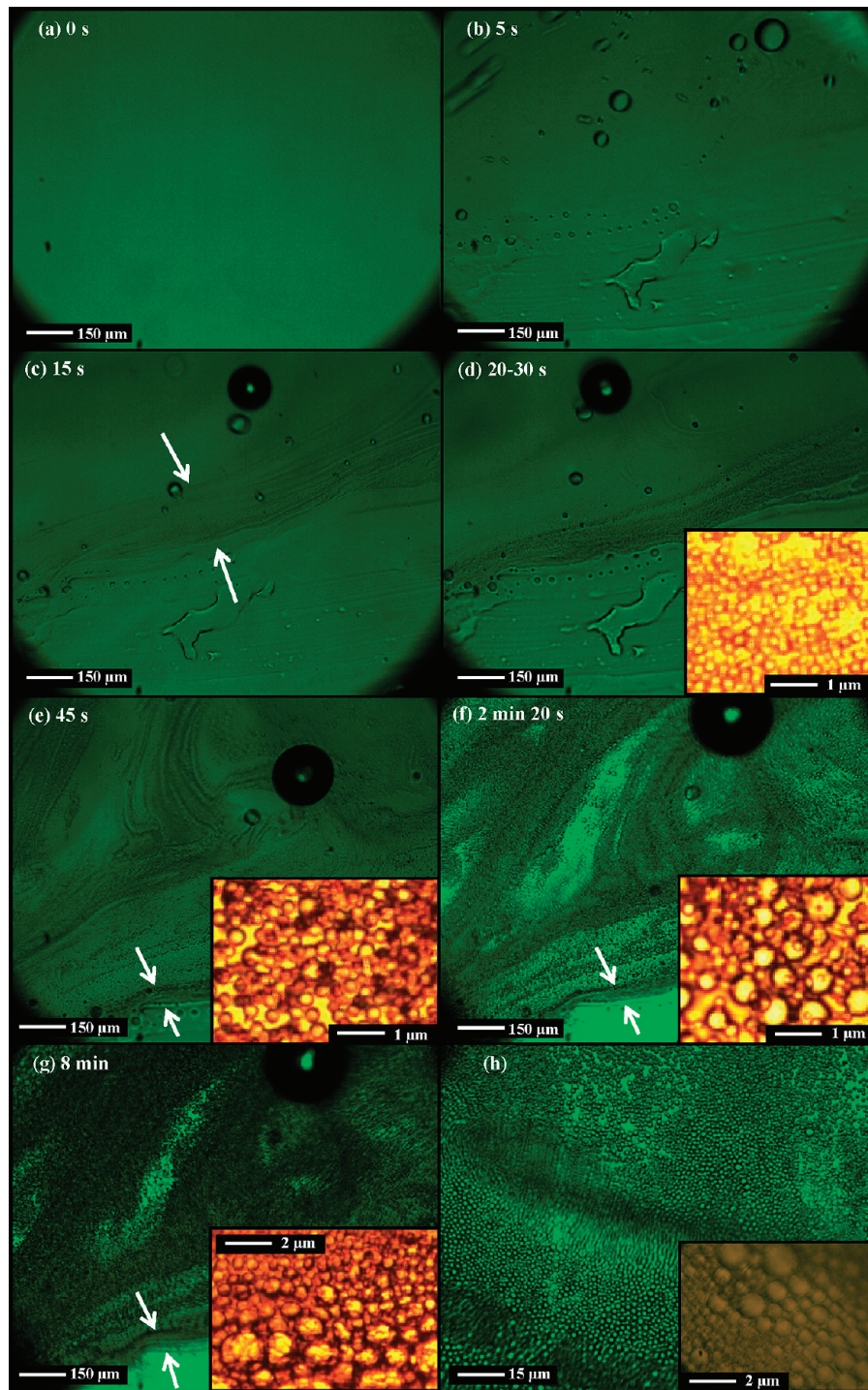


**Figure 9.** OM sequential images of Al—Si ester/TMOS (molar ratio 1:1) mixture in contact with a aqueous alkaline solution ( $\text{pH} = 13.0$ ) for different time values.

inside the inorganic phase, until the whole system freezes due to the extension of polycondensation reactions. In about 2 min (Figure 9f), the inorganic jelly phase is so viscous that bubbles are immobilized inside the structure, thus limiting their size to around 1–2  $\mu\text{m}$  large and preventing their coalescence into one unique macroscopic liquid phase. These observations are in perfect agreement with the SEM and TEM observations. Until approximately 8 min (Figure 9g), some more droplets of liquid still appear slowly, involving a darker structure, fully

riddled of these regular bubbles. Figure 9h shows bubbles at different magnification scales. Figure 10 summarizes these time-dependent OM observations. The formation mechanism could thus be established as follows: When the di-*s*-butoxyaluminoxytriethoxysilane and silica coreactant mixture is added dropwise to the aqueous media, a rapid polymerization occurs, which induces a sudden release of alcohol and water molecules, resulting from hydrolysis (1,2) and condensation (3,4,5) reactions

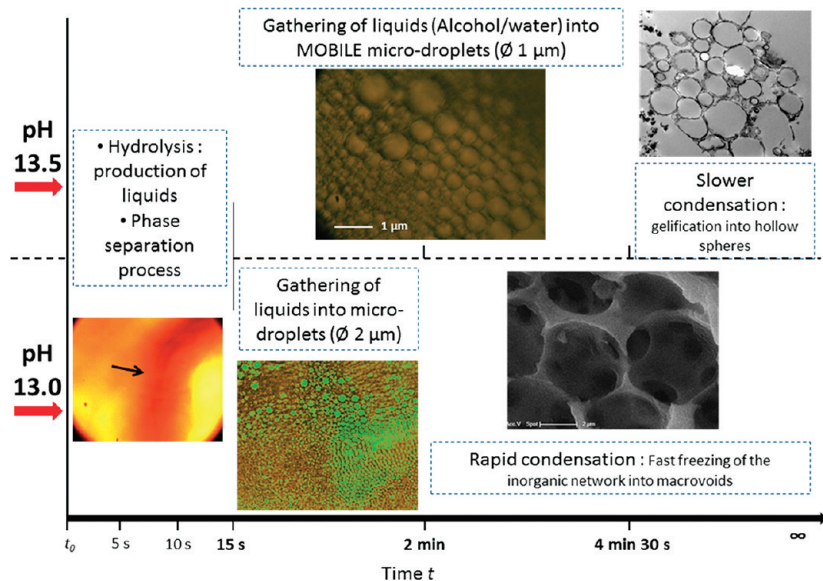
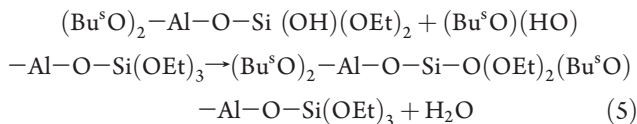
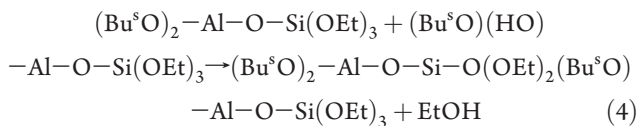
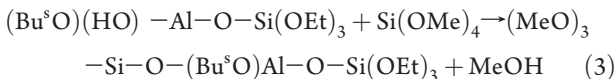
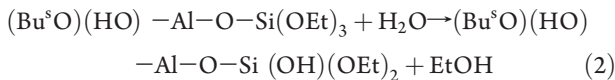
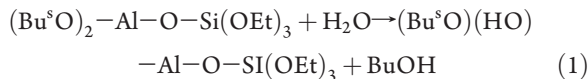


**Figure 10.** Summary scheme of the OM-based observations on the Al–Si ester/TMOS mixture polymerization on pH 13.0 (down) and 13.5 (up) alkaline film.



Due to the high reactivity of Al alkoxide functionality, hydrolysis and condensation reactions begin from its side (reactions 1, 3, and 4), although high alkaline conditions can favor the hydrolysis and condensations of the alkoxy silane side (reaction 2). As the reaction progresses, more and more liquid molecules (i.e., MeOH, EtOH, BuOH, and water) are generated inside the particle. The rapid self-aggregation and condensation of aluminosilicate nanoparticles coupled with the rapid release of water/alcohol spherical drops simultaneously occur to form a jelly structure. This might produce, at the earlier stage of the polymerization process, microphase-separated domains of the phase formed by aluminosilicate-based nanoparticles and water/alcohol microspheres. The jelly structure, constructed by nanoparticles, would thus freeze throughout the conversion of liquid precursors into solid oxides. After removal of solvent by drying, a highly spongy

macroporous particle with macrovoids throughout the solid body is formed.

It is worthy to note that the macropores formed in the present case from the polymerization of the Al–Si ester/TMOS mixture are very different from meso–macroporous aluminosilicates synthesized with the mixture of  $\text{Al(OBu)}_3$ /TMOS, characterized by tubular macrochannels, approximately parallel to each other and perpendicular to the surface of the monolithic particle (Figure 8). These relatively straight tubes extended throughout the whole particle. In our present case, the aluminosilicate skeleton is riddled of micrometer-sized spherical voids ( $1\text{--}2\ \mu\text{m}$  in diameter). In addition, the walls are thinner than those encountered with other metal alkoxides. These morphological parameters arise from the combination of the utilization of a single molecular precursor bearing a less reactive alkoxy silane function and the addition of tetramethoxysilane, which could affect this macroporosity by a drastic diminution of the conversion rate of liquid alkoxides into solid oxides. This fact has a major consequence. When pure metal alkoxides are carried into an aqueous solution by a dropwise addition, the very fast transformation of hydrophobic metal alkoxide into metal oxide permits the freezing and the contraction of the external crust of the droplet during the polymerization process. The small droplet shape generates an important curved surface, which is applying some core-directed pressures on the water/alcohol microdroplets contained in the near surface of the metal alkoxide particle. The microdroplets are consequently pushed straight toward the center of the droplet, where the inorganic precursor remains unreacted and opposes less resistance to the front of the solvents.<sup>3</sup> This pressure should be a driving force responsible for the straight shaped macrostructure. It should be important to indicate that, whatever the preparation conditions are, metal alkoxides, due to their elevated reactivity (high hydrolysis and polycondensation rates in aqueous solution), can lead to the formation of a meso–macroporous structure with parallel straight macrochannels organization.<sup>3–5,7,12,14,15</sup> Whereas, when the Al–Si ester is

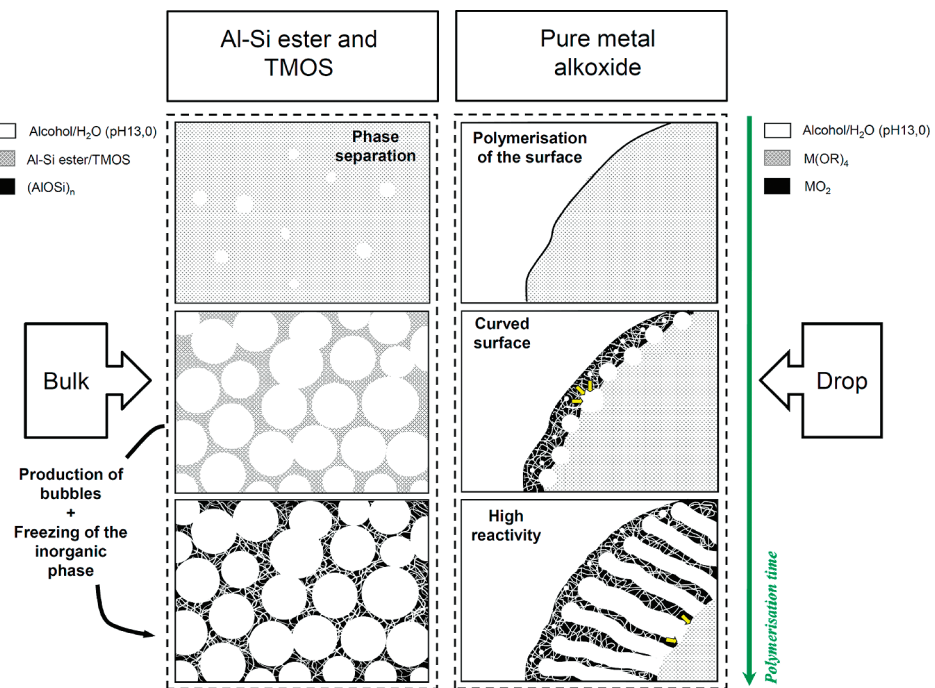


**Figure 11.** Comparative scheme of the macroporous construction between the pure metal alkoxide's way (right) and the "single drop" single bifunctional precursor/silica coreactant mixture's way (left).

mixed with TMOS, alkoxy bridging occurs in the coordination sphere of the highly reactive aluminum part of the single molecular precursor, and thus subsequent polymerization is more gradual and homogeneous. Even in the case of a very low dropwise addition, all the droplets of this mixture gather to form one unique homogeneous gelatinous cloud. This is certainly the alkoxysilane coreactant contribution to the improvement of the solubility of the inorganic mixture since individually used Al—Si ester leads to independent droplets. In this "single drop", the surface/volume ratio is less important, and no driving forces are applied to the microdroplets of solvents. Thus, the inorganic aluminosilicate material surrounding the liquid droplets slowly hardens, which enables the slow formation of mobile, regular, and independent microdroplets which stay in the static spherical shaped configuration during the whole polymerization process. The scheme in Figure 11 summarizes this proposal with a comparative diagram between the pure metal alkoxide and the Al—Si ester/TMOS mixture pathways.

Significant modifications in both morphology and textural properties were observed when pH value increased from pH = 13.0 to 13.5. The Al—Si—TM13 material obtained at pH = 13.0 (Figures 3c and 4c) featured particles fully riddled with interconnected regular micrometer-sized and spherically shaped macrovoids separated by very thin mesoporous walls, while particles of Al—Si—TM13.5 material synthesized at pH = 13.5 (Figures 3d and 4d) consist of the stacking of regular microsized (1–2  $\mu\text{m}$  in diameter) fragile hollow spheres, although it is difficult to explain why a huge modification took place with such a slight increase in pH value. From our study, it can be suggested that it is probably due to the modification of hydrodynamics of the system. In fact, it is observed by MO that at pH 13.5 the liquid (alcohol/water molecules) microdroplets formed inside the aluminosilicate phase (Al—Si ester/TMOS mixture) remain

mobile for a longer period of time (up to 4 min), while in the case of pH 13.0, microdroplets become frozen 2 min after the contact of the Al—Si ester/TMOS mixture and water. This difference in the gelification time could confer a higher mobility to the emulsion of the microdroplets, resulting in independent hollow spheres. Figure 12 gives a schematic representation describing the difference in the abundance and the morphology of the meso—macroporous aluminosilicate particles from synthesis at pH 13.0 and 13.5.

Without the additional silica precursor, the formation of a macroporous scaffold results, due to higher polymerization rates, in some irregular and rare cavities. Another observation is that only pH values of 13.0 and 13.5 are more favorable for the generation of macroporosity into the aluminosilicate particles than for other pH values. Under more acidic or more basic conditions, no such macroporous particles form. This observation is supported by optical imaging (Figure 13) of Al—Si ester/TMOS mixture droplets in solution at different pH values (2.0, 6.5, 13.0, and 13.5). These images show that for pH = 13.0 and 13.5 solutions (Figure 13c and d, respectively) an extremely high number of liquid microdroplets ( $\text{H}_2\text{O}$ , alcohol) at the origin of the macrostructure, resulting from the hydrolysis of inorganic precursors, are confined into the jellified inorganic phase. This is evidently not the case for other pH synthetic medias (Figure 13a and b) for which no microbubbles are observed within the aluminosilicate inorganic phase in gelification. Some major parameters which are affected by the variation of the pH are the solubility of inorganic species, their charge density, and their rate of polymerization. Hence, the rate of polymerization is one of the key parameters affecting the hydrodynamic environment and subsequently the development of the macroporous scaffold. There is a direct relationship between the microbubbles formed in the Al—Si ester/TMOS phase and the spherically shaped macrostructure observed by TEM and SEM.

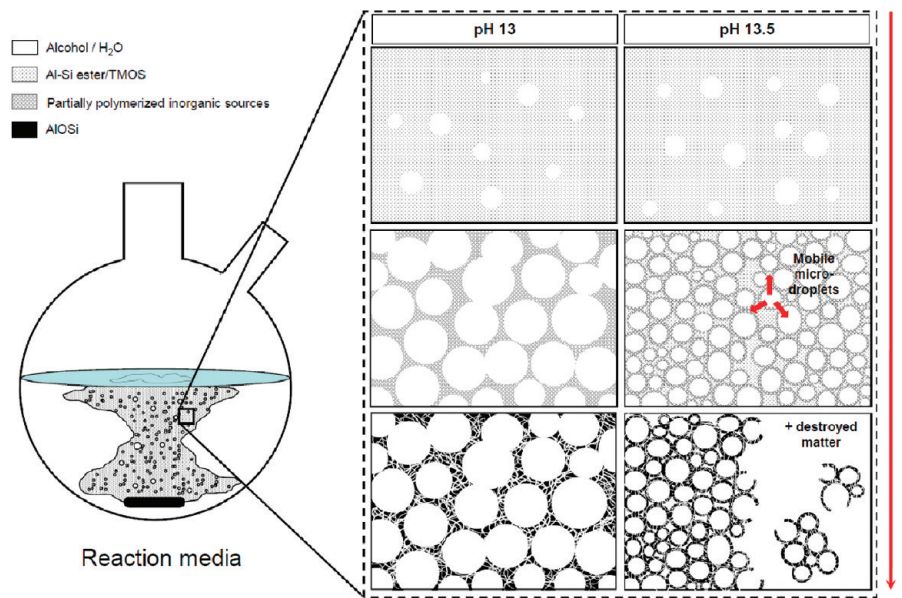


**Figure 12.** Comparative scheme summarizing the different possible process occurring between materials synthesized from pH of 13.0 (left) and 13.5 (right) during the polymerization of the Al—Si ester/TMOS mixtures.

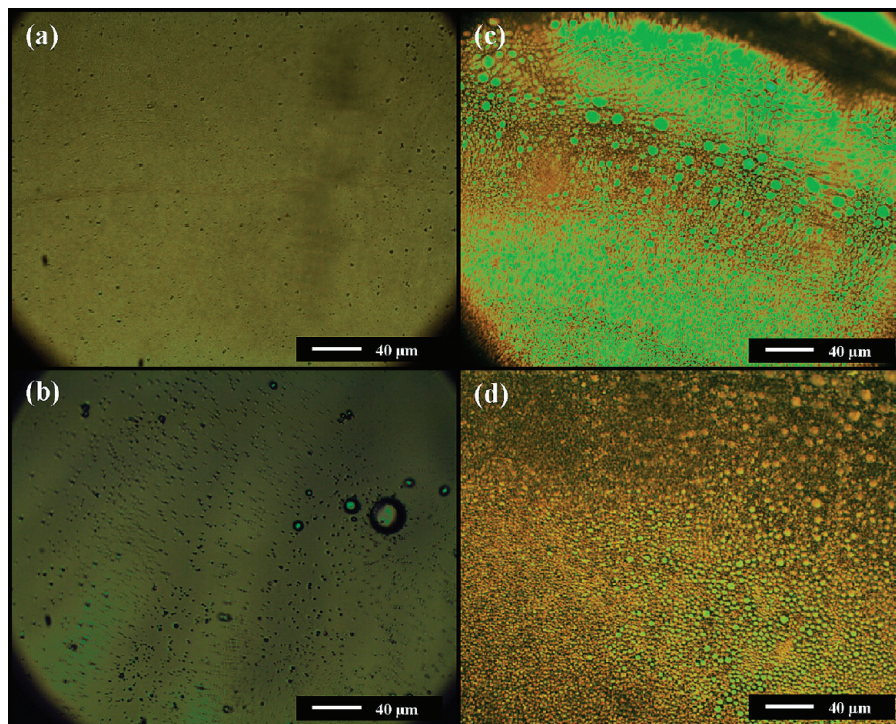


**Figure 13.** OM images of Al—Si ester/TMOS droplets dropped off on a water film at different pH values: (a) pH = 2.0, (b) pH = 6.5, (c) pH = 13.0, and (d) pH 13.5 after 10 min of polymerization.

#### 4. CONCLUSIONS

On the basis of a detailed optimization study using the single-source molecular alkoxide precursor  $(sec\text{-OBu})_2\text{-Al-O-Si-(OEt)}_3$ , hierarchically structured 3D meso—macroporous aluminosilicate materials, containing a higher level of tetrahedral aluminum, were successfully synthesized via the mixing of the single-source molecular alkoxide precursor and an inorganic silica coreactant, the TMOS. The use of this silica coreagent was studied

at different pH values. Under these conditions, when the silica precursor is thoroughly mixed with di-*s*-butoxyaluminooxytriethoxysilane before a dropwise addition into aqueous solutions, a major phenomenon can be observed. In addition to the improvement of heterocondensation reactions between the hydrolytic aluminum-alkoxide part of  $(sec\text{-OBu})_2\text{-Al-O-Si-(OEt)}_3$  and the silica coreagent alkoxide functional groups, resulting in a significant increased amount of tetrahedral aluminum atoms incorporated

into the aluminosilicate framework, the mixing produces a spontaneously unusual 3D meso-macroporous scaffold, which is very different from the straight macrochannels observed in materials synthesized from separated aluminum and silica alkoxide precursors or pure metal alkoxide precursors. This byproduct templated macrostructure self-formation phenomenon was directly observed by *in situ* optical microscopy. There exists a direct correlation between the microbubbles formed in the synthesis droplet and the macrostructure observed by SEM and TEM. A formation mechanism has been consequently proposed. The high hydrolysis and polycondensation rates of di-*s*-butoxyaluminoxylithoxysilane combined with the less reactive TMOS induce the important release of liquid byproduct (water and alcohol). These byproduct liquids are gathering, via a phase separation, to form, at pH of 13.0–13.5, a very homogeneous dispersion of an extremely high number of microsized microbubbles which act as a liquid porogen during the freezing of the aluminosilicate phase. This phenomenon of emulsion and the stabilization of homogeneous spherically shaped porogen byproduct microbubbles was rendered possible due to a very subtle equilibrium between a precise polymerization rate of the inorganic precursors and the formation of a unique viscous aluminosilicate phase, destitute of high surfacial pressures. It was clearly stated, by the combination of multiple characterization techniques, that the emergence of the homogeneous microbubble dispersion can be directly correlated to the typical spherically shaped macrostructure observed within the aluminosilicate matrixes. A mixture of Al–Si ester/TMOS at pH of 13.0 yields particles penetrated by numerous regular micrometer-sized spherical interconnected macrovoids. These macropores are separated by very thin wormhole-like mesoporous walls. A slight rise of the basicity (pH = 13.5) of the synthesis media influences both the incorporation of aluminum into a tetrahedral environment and the morphology of the macrostructure. Indeed, due to a lower gelification process, liquid byproduct microbubbles are more mobile in the aluminosilicate phase, resulting in the generation of the stacking of independent hollow mesoporous spheres of 1 μm large. Observations obtained via optical microscopic investigations lead to a proposal of macrostructure mechanistic formation and contribute to bringing highly valuable information in the field of hierarchical meso-macroporosity self-formation phenomena. This work also provides a versatile synthesis route to materials with advanced functionality. With this synthesis procedure, not only can we synthesize different meso-macroporous aluminosilicates with different Si/Al ratios but also instead of  $(\text{sec-BuO})_2\text{-Al-O-Si(OEt)}_3$ , it is possible to synthesize hierarchically structured meso-macroporous titanosilicates or zirconosilicates by using other single molecular precursors such as  $\text{Zr}[\text{OSi(O}_t\text{-BuO)}_3]_4$  or  $\text{Ti}[\text{OSi(O}_t\text{-BuO)}_3]_4$ .

## AUTHOR INFORMATION

### Corresponding Author

\*Email: bao-lian.su@fundp.ac.be. Tel.: +32-81-724531. Fax: +32-81-72-54-14. Or baoliansu@whut.edu.cn. Tel.: + 86-27-87-85-53-22.

## ACKNOWLEDGMENT

A. Lemaire thanks the Belgian FNRS (Fonds National de la Recherche Scientifique) for his Research Fellow position. This work was realized in the frame of Inanomat, a Belgian federal government (Belspo) PAI-IUAP (6/17) project, and an Interreg IV (France-Wallonia) “Redugaz” project financially supported

by the European Community and Wallonia region. B. L. Su acknowledges the Chinese Central Government for an “Expert of the State” position in the program of “Thousands Talents” and the Chinese Ministry of Education for a “Changjiang Scholar” position at the Wuhan University of Technology.

## REFERENCES

- (1) (a) Chen, X.; Wang, X.; Fu, X. *Energy Environ. Sci.* **2009**, *2*, 872. (b) Idakiev, V.; Tabakova, T.; Yuan, Z. Y.; Su, B. L. *Appl. Catal., A* **2004**, *270*, 135. (c) Idakiev, V.; Tabakova, T.; Naydenov, A.; Yuan, Z. Y.; Su, B. L. *Appl. Catal., B* **2006**, *63*, 178. (d) Tidahy, H. L.; Siffert, S.; Lamontier, J. F.; Zhilinskaya, E.; Aboukais, A.; Yuan, Z. Y.; Vantomme, A.; Su, B. L.; Canet, X.; De Weireld, G.; Frere, M.; N'Guyen, T.; Giraudon, J.; Leclercq, G. *Appl. Catal., A* **2006**, *310*, 61. (e) Hosseini, M.; Siffert, S.; Tidahy, H. L.; Cousin, R.; Lamontier, J.; Aboukais, A.; Vantomme, A.; Roussel, M.; Su, B. L. *Catal. Today* **2007**, *122*, 391. (f) Yuan, Z. Y.; Idakiev, V.; Vantomme, A.; Tabakova, T.; Ren, T. Z.; Su, B. L. *Catal. Today* **2008**, *131*, 203. (g) Tidahy, H. L.; Hosseini, M.; Siffert, S.; Cousin, R.; Lamontier, J. F.; Aboukais, A.; Su, B. L.; Giraudon, J. M.; Leclercq, G. *Catal. Today* **2008**, *137*, 335. (h) Giraudon, J. M.; Nguyen, T. B.; Leclercq, G.; Siffert, S.; Lamontier, J. F.; Aboukais, A.; Vantomme, A.; Su, B. L. *Catal. Today* **2008**, *137*, 379. (i) Zeng, T.; Zhou, Z.; Zhu, J.; Cheng, Z.; Yuan, P.; Yuan, W. *Catal. Today* **2009**, *147*, 41. (j) Cao, J.; Shao, G.; Ma, T.; Wang, Y.; Ren, T.; Wu, S.; Yuan, Z. *J. Mater. Sci.* **2009**, *44*, 6717. (k) Zhou, Z.; Zeng, T.; Cheng, Z.; Yuan, W. *Ind. Eng. Chem. Res.* **2010**, *49*, 11112. (l) Ho, C.; Yu, J. C.; Wang, X.; Lai, S.; Qiu, Y. *J. Mater. Chem.* **2005**, *15*, 2193. (m) Wang, G.; Coppens, M. *Chem. Eng. Sci.* **2010**, *65*, 2344.
- (2) (a) Maekawa, H.; Esquena, J.; Bishop, S.; Solans, C.; Chmelka, B. F. *Adv. Mater.* **2003**, *15*, 591. (b) Chen, H. R.; Gu, J. L.; Shi, J. L. *Adv. Mater.* **2005**, *17*, 2005. (c) Backov, R. *Soft Matter* **2006**, *2*, 452. (d) Yang, P.; Deng, T.; Zhao, D.; Feng, P.; Pine, D.; Chmelka, B. F.; Whitesides, G. M.; Stucky, G. D. *Science* **1998**, *282*, 2244. (e) Pega, S.; Boissière, C.; Grossi, D.; Azaïs, T.; Chaumonnot, A.; Sanchez, C. *Angew. Chem., Int. Ed.* **2009**, *48*, 2784. (f) Carn, F.; Steunou, N.; Livage, J.; Backov, R. *Chem. Mater.* **2005**, *17*, 644. (g) On, D. T.; Kaliaguine, S. *Angew. Chem., Int. Ed.* **2001**, *40*, 3248. (h) On, D. T.; Kaliaguine, S. *Angew. Chem., Int. Ed.* **2002**, *41*, 1036. (i) Way, J.; Yue, W.; Zhou, W.; Coppens, M. O. *Microporous Mesoporous Mater.* **2008**, *120*, 19. (j) Valtchev, V. P.; Smalhi, M.; Faust, A. C.; Vidal, L. *Chem. Mater.* **2004**, *16*, 1350. (k) Caruso, R. A.; Antonietti, M. *Adv. Funct. Mater.* **2002**, *12*, 307. (l) Valtchev, V.; Smalhi, M.; Faust, A. C.; Vidal, L. *Angew. Chem., Int. Ed.* **2003**, *42*, 2782. (m) Amatani, T.; Nakanishi, K.; Hirao, K.; Kodaira, T. *Chem. Mater.* **2005**, *17*, 2114. (n) Zeng, T.; Zhou, Z.; Zhu, J.; Cheng, Z.; Yuan, P.; Yuan, W. *Catal. Today* **2009**, *147*, 41. (o) Chen, X.; Wang, X.; Fu, X. *Energy Environ. Sci.* **2009**, *2*, 872. (p) Wang, G.; Coppens, M. O. *Chem. Eng. Sci.* **2010**, *65*, 2344.
- (3) (a) Léonard, A.; Su, B. L. *Colloids Surf., A* **2007**, *300*, 129. (b) Vantomme, A.; Léonard, A.; Yuan, Z. Y.; Su, B. L. *Colloids Surf., A* **2007**, *300*, 70. (c) Dapsens, P. Y.; Hakim, S. H.; Su, B. L.; Shanks, B. H. *Chem. Commun.* **2010**, *46*, 8980.
- (4) Su, B. L.; Léonard, A.; Yuan, Z. Y. *C. R. Chim.* **2005**, *8*, 713.
- (5) (a) Léonard, A.; Blin, J. L.; Su, B. L. *Chem. Commun.* **2003**, 2568. (b) Léonard, A.; Su, B. L. *Chem. Commun.* **2004**, 1674.
- (6) (a) Judith, E. G.; Wijnhoven, J.; Vos, W. L. *Science* **1997**, *281*, 802. (b) Holland, B. T.; Blanford, C. F.; Stein, A. *Science* **1998**, *281*, 538. (c) Jiang, P.; Bertone, J. F.; Colvin, V. L. *Science* **2001**, *291*, 453.
- (7) Yuan, Z. Y.; Blin, J. L.; Su, B. L. *Chem. Commun.* **2002**, 504.
- (8) (a) Zhang, B.; Davis, S. A.; Mann, S. *Chem. Mater.* **2002**, *14*, 1369. (b) Walsh, D.; Arcelli, L.; Ikoma, T.; Tanaka, J.; Mann, S. *Nat. Mater.* **2003**, *2*, 386. (c) Kataoka, K.; Nagao, Y.; Nukui, T.; Akiyama, I.; Tsuru, K.; Hayakawa, S.; Osaka, A.; Huh, N. H. *Biomaterials* **2005**, *26*, 2509.
- (9) (a) Wu, M.; Fujii, T.; Messing, G. L. *J. Non-Cryst. Solids* **1990**, *121*, 407. (b) Carn, F.; Colin, A.; Achard, M.-F.; Deleuze, H.; Saadi, Z.; Backov, R. *Adv. Mater.* **2004**, *16*, 140. (c) Chandrappa, G. T.; Steunou, N.; Livage, J. *Nature* **2002**, *416*, 702.

(10) (a) Imhof, A.; Pine, D. J. *Nature* **1997**, *389*, 948. (b) Imhof, A.; Pine, D. J. *Adv. Mater.* **1998**, *10*, 697.

(11) Nishihara, H.; Mukai, S. R.; Yamashita, D.; Tamon, H. *Chem. Mater.* **2005**, *17*, 683.

(12) Yuan, Z. Y.; Su, B. L. *J. Mater. Chem.* **2006**, *16*, 663.

(13) S Davis, S. A.; Burkett, S. L.; Mendelson, N. H.; Mann, S. *Nature* **1997**, *385*, 420.

(14) (a) Ren, T. Z.; Yuan, Z. Y.; Su, B. L. *Chem. Commun.* **2004**, 2730. (b) Deng, W.; Toepke, M. W.; Shanks, B. H. *Adv. Funct. Mater.* **2003**, *13*, 61. (c) Deng, W.; Shanks, B. H. *Chem. Mater.* **2005**, *17*, 3092.

(d) Hakin, S. H.; Shanks, B. H. *Chem. Mater.* **2009**, *21*, 2027. (e) Collins,

A.; Carriazo, D.; Davis, S. A.; Mann, S. *Chem. Commun.* **2004**, 568. (f)

Yuan, Z. Y.; Ren, T. Z.; Vantomme, A.; Su, B. L. *Chem. Mater.* **2004**, *16*, 5096. (g) Su, B. L.; Vantomme, A.; Surahy, L.; Pirard, R.; Pirard, J. P.

*Chem. Mater.* **2007**, *19*, 3325. (h) Yang, X. Y.; Li, Y.; Van Tendeloo, G.;

Xiao, F. S.; Su, B. L. *Adv. Mater.* **2009**, *21*, 1368. (i) Yang, X. Y.; Li, Y.;

Lemaire, A.; Yu, J. G.; Su, B. L. *Pure Appl. Chem.* **2009**, *81*, 2265.

(15) (a) Yuan, Z. Y.; Ren, T. Z.; Azioune, A.; Pireaux, J. J.; Su, B. L.

*Chem. Mater.* **2006**, *18*, 1753. (b) Ren, T. Z.; Yuan, Z. Y.; Su, B. L.

*Langmuir* **2004**, *20*, 1531. (c) Blin, J. L.; Léonard, A.; Yuan, Z. Y.; Gigot,

L.; Vantomme, A.; Cheetam, A. K.; Su, B. L. *Angew. Chem., Int. Ed.* **2003**,

*42*, 2872. (d) Vantomme, A.; Yuan, Z. Y.; Su, B. L. *New J. Chem.* **2004**, *28*,

1083. (e) Yuan, Z. Y.; Vantomme, A.; Léonard, A.; Su, B. L. *Chem.*

*Commun.* **2003**, 1558. (f) Yuan, Z. Y.; Ren, T. Z.; Su, B. L. *Adv. Mater.*

**2003**, *15*, 1462. (g) Ren, T. Z.; Yuan, Z. Y.; Su, B. L. *Chem. Phys. Lett.*

**2004**, *388*, 46. (h) Yuan, Z. Y.; Ren, T. Z.; Azioune, A.; Pireaux, J. J.; Su,

B. L. *Catal. Today* **2005**, *105*, 647.

(16) Li, Y.; Yang, X. Y.; Tian, G.; Vantomme, A.; Yu, J. G.; Van Tendeloo, G.; Su, B. L. *Chem. Mater.* **2010**, *22*, 325.

(17) (a) Yang, X. Y.; Vantomme, A.; Lemaire, A.; Xiao, F. S.; Su, B. L. *Adv. Mater.* **2006**, *18*, 2117. (b) Lemaire, A.; Su, B. L. *Langmuir* **2010**, *26*, 17603.

(18) Lemaire, A.; Su, B. L. *Micro. Meso. Mater.* **2010**, 10.1016/j.micromeso.2010.11.019.

(19) Brinker, C. J.; Scherer, G. W. *Sol-Gel Science, The Physics and Chemistry of Sol-Gel Processing*; Academic Press Inc.: San Diego, 1999.

(20) Blin, J. L.; Léonard, A.; Su, B. L. *Chem. Mater.* **2001**, *13*, 3542.

(21) (a) Lippmaa, E.; Mägi, M.; Samoson, A.; Tarmak, M.; Engelhardt, G. *J. Am. Chem. Soc.* **1981**, *103*, 4992. (b) Ferchiche, S.; Valcheva-Traykova, M.; Vaughan, D. E. W.; Warzywoda, J.; Socco, A., Jr.

*J. Cryst. Growth* **2001**, *222*, 801. (c) Lippmaa, E.; Samoson, A.; Magi, M.

*J. Am. Chem. Soc.* **1986**, *108*, 1730.